Catalysis Today 141 (2009) 43–51

Contents lists available at ScienceDirect

Catalysis Today

journal homepage: www.elsevier.com/locate/cattod

Design and development of Ti-modified zeolite-based catalyst for hydrocracking heavy petroleum☆

Hiromichi Shimada [a,*], Koichi Sato [a], Kosaku Honna [b], Toshiyuki Enomoto [b], Nobuyasu Ohshio [b]

[a] National Institute of Advanced Industrial Science and Technology (AIST), 1-1-1 Higashi, Tsukuba, Ibaraki 305-8565, Japan
[b] Japan Corporation Center for Petroleum, Sunshine Building 58F, 3-1-1 Higashi-Ikebukuro, Toshima, Tokyo 170-6058, Japan

ARTICLE INFO

Article history:
Available online 2 June 2008

Keywords:
NiMo sulfide catalyst
Mesoporosity
Acidity
Hydrogenation
Catalyst deactivation

ABSTRACT

New Ni–Mo sulfide catalysts with zeolite-based supports were designed and developed for hydrocracking heavy petroleum to meet the increasing demand for transportation fuels. The supports consisted of modified ultra-stable-Y zeolite (MTZ) and an Al_2O_3 binder. The MTZ was prepared by immersing ultra-stable-Y zeolite in aqueous $Ti(SO_4)_2$ solutions, followed by Mo loading with the equilibrium adsorption of ammonium heptamolybdate. The catalytic performance of NiMo/MTZ, prepared by one-step incipient wetness impregnation of the MTZ support, was then evaluated using a bench-scale plant with a fixed-bed reactor. NiMo/MTZ showed high AR conversion, high selectivity to middle distillate (MD) fraction, and almost no deactivation up to 2600 h. This high performance was attributed to the large mesoporosity and controlled acidity of MTZ.

1. Introduction

According to the reference scenario by the International Energy Agency [1], the world primary energy demand in 2030 will be more than 50% higher than that in 2005, reaching 17.7 billion tons of oil equivalent (Btoe), compared with 11.4 Btoe in 2005. Fossil fuel will remain the dominant source for primary energy and petroleum will be the single largest fuel, although the contribution from petroleum will decrease slightly. The contribution from other fossil fuels, such as coal and natural gas, will increase for power generation. However, the contribution from petroleum will continue to dominate for transportation, although it is expected to slightly decrease from 94% in 2005 to 92% in 2030 due to the increase in the contribution from biofuels.

The total production of conventional and unconventional crude oil and non-conventional oil from gas-to-liquids (GTL) in 2006 was 36 mbbl/d. The demand for total oil will reach 61 mbbl/d in 2030 [1]. World oil reserves are sufficient to meet the projected growth in the demand up to 2030, provided that the contribution by GTL and unconventional crude oil such as oil sands is increased. In this context, the technological development to produce transportation fuel from resources other than conventional crude oil is one of the most urgent energy issues that need to be resolved. Catalytic science and technology must play important roles in this development in various technological fields, such as biofuel production, GTL production, or unconventional oil refining. The present paper introduces our project to develop a new hydrocracking catalyst for heavy petroleum. The primary target of the project is to obtain distillates from atmospheric residue (AR) in conventional crude oil, but the developed catalysts can be easily applied to variety of heavy hydrocarbon feedstocks including oil sand bitumen.

Several technologies to produce more transportation fuels from heavy fractions of petroleum have been investigated. Heavy oil hydrocracking is a promising technology in terms of efficiency, because compared to coking processes or thermal cracking processes, this process yields high selectivity to middle distillate (MD, diesel and jet fuels) and low selectivity to coke [2–4]. In most cases, hydrocracking is combined with other pretreatment processes such as solvent deasphalting or mild hydrotreating. Even after these pretreatment processes, the feedstocks for hydrocracking processes are so heavy that conventional acid catalysts are easily deactivated by catalyst poisons contained in the feedstocks. Catalysts must therefore possess both hydrocracking activity and high durability against catalyst poisons such as polyaromatics, basic compounds, and metallic elements.

In the present study, Ni–Mo sulfide was chosen as the hydrogenation active component and Y zeolite as the acidic component. Ni–Mo was chosen due to its higher hydrogenation activity compared with Co–Mo, and Y zeolite was chosen because compared with amorphous silica alumina or other mixed oxides,

☆ This forms part of the plenary lecture delivered in the symposium.
* Corresponding author.
E-mail address: h-shimada@aist.go.jp (H. Shimada).

0920-5861/$ – see front matter © 2008 Elsevier B.V. All rights reserved.
doi:10.1016/j.cattod.2008.04.012

the acid sites in the crystalline aluminosilicates of Y zeolite are with relatively even acid strength and the density of the acid sites is easy to control. In fact, compared with other zeolites, Y zeolites exhibit superior performance in hydrocracking petroleum [2,5–9]. This superior performance of Y zeolite is due to the abundant mesopores ($D > 2$ nm) and to the appropriate acid density and strength that can be controlled by changing the Si/Al ratio.

In the present study, the properties of Y zeolite were improved so that zeolite-based catalysts could achieve high performance, including a longer catalyst life in the hydrocracking of heavy petroleum. First, we modified ultra-stable-Y (USY) zeolite powders with $Ti(SO_4)_2$ aqueous solutions [10]. After confirming the catalytic performances of the modified Y zeolite, we then prepared practical catalysts by impregnating Ni and Mo on the extrudate-type support made from this modified zeolite powder and a γ-Al_2O_3 binder. Finally, we evaluated the catalytic activity and catalyst life up to 2600 h of the Ni and Mo loaded extrudate-type catalysts by using a bench-scale reactor.

2. Design of Ti-modified zeolite catalyst (TZ catalyst)

2.1. Extraction of Al from the zeolite framework

Hydrothermally synthesized NaY zeolites have relatively low Si/Al ratios (<3). The following procedure to prepare HY zeolites with ion exchange (IE) of Na^+ by NH_4^+ in acidic solutions, such as $(NH_4)_2SO_4$, simultaneously caused the extraction of Al from the zeolite framework. Table 1 [11] shows the change in chemical composition of Y zeolite with IE by using an $(NH_4)_2SO_4$ aqueous solution. With increasing cycles of IE, the Al content in the framework decreased (note that the relative crystallinity and surface area did not significantly decrease).

The mesopore volume also increased with increasing IE (Table 1). Mesopores were likely formed during the calcination procedures after IE and the washing and drying procedures, when the Al-deficient framework was stabilized. Fig. 1 [11] compares the pore distribution profiles of Y zeolites before and after IE. The profiles of ion-exchanged Y zeolites show that mesopores about 4 nm in diameter were formed and then grew with increasing cycles of IE (here, IE1, IE2, and IE3 is the zeolite after one, two, and three ion exchanges, respectively).

To further increase the mesoporosity and decrease the acidity, HY zeolites are often subject to steaming or acid treatment. Thus prepared zeolites by steaming or acid treatment, often called ultra-stable-Y (USY) zeolites, exhibit high mesoporosity and low acidity. As the starting material for the zeolite in the present study, we chose a commercially available USY zeolite (USY1, Tosoh, HSZ-330HUA). $Ti(SO_4)_2$ modification conditions were investigated as follows: $Ti(SO_4)_2$ concentration (0.05–0.20 mol/L), temperature (25 or 50 °C), time (0.17–4 h). Table 2 [13] shows the properties of two $Ti(SO_4)_2$ modified zeolite catalysts (TZ catalysts) that exhibited superior performance in the following catalytic activity tests in Table 4. The $Ti(SO_4)_2$ modification of USY1 zeolite further extracted the remaining Al from the framework of USY1 as shown by the decrease in the acidity with a slight decrease in the crystallinity. Fig. 2 [13] shows the NH_3-TPD spectra of the starting USY zeolites and a TZ catalyst. The $Ti(SO_4)_2$ modification reduced both the high-temperature and low-temperature peaks. The high-temperature peaks at about 350 °C can be assigned to the "zeolitic" acid sites arising from the framework of zeolite, whereas the low-temperature peaks at about 200 °C can be assigned to the acid sites originating from the extra-framework Al (see Section 2.2). Note that USY2 with a high Si/Al ratio (>100) did not exhibit acidity.

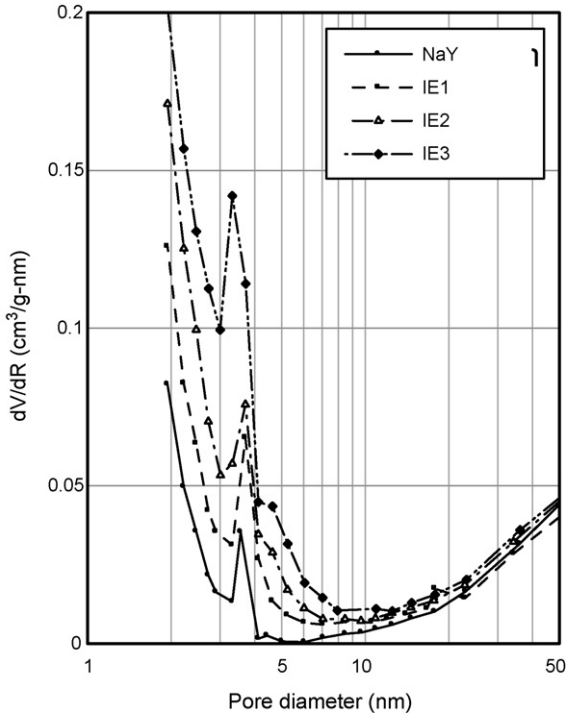

Fig. 1. Change in pore size distribution of Y zeolite after one, two, and three ion exchanges (IE1, IE2, and IE3, respectively). Na form: original NaY zeolite.

Table 1
Changes in chemical composition and physical properties of Y zeolites with ion exchange

	Na (wt%)	Si/Al_{fw}[a]	Si/Al_{bk}[b]	S.A.[c] (m^2/g)	Meso PV[d] (cm^3/g)	R.C.[e] (%)
NaY[f]	7.1	2.8	2.8	753	0.068	100
IE 1[f]	2.6	2.8	2.8	724	0.077	86
IE 2[f]	0.7	4.1	3.2	748	0.093	84
IE 3[f]	0.3	5.0	3.2	766	0.114	80

[a] Si/Al ratio of zeolite framework using XRD data and Breck's equation [12].
[b] Si/Al ratio of bulk zeolite determined by ICP emission spectroscopy.
[c] BET surface area.
[d] Mesopore volume obtained by N_2 adsorption and *t*-plot method.
[e] Relative crystallinity obtained by the total intensity of the six XRD peaks according to ASTM D3906.
[f] NaY was a commercially available NaY zeolite (Tosoh Co.). IE1, IE2 and IE 3 were HY zeolites, respectively, after first, second and third ion exchange of NaY with $(NH_4)_2SO_4$.

Table 2
Chemical composition and physical properties of USY and $Ti(SO_4)_2$ modified zeolites (TZ)

	Si/Al	TiO_2 (%)	S.A. (m^2/g)	Meso PV (cm^3/g)	R.C. (%)	Acidity[a] (mmol/g)
USY1[b]	3.2	–	626	0.136	87	0.8
USY2[b]	125	–	677	0.248	101	0.00
TZ5[c]	40	7.8	803	0.170	43	0.26
TZ6[c]	15	9.1	833	0.186	65	0.45

[a] Acidity here was "zeolitic acidity" determined using the NH_3-TPD method. NH_3-TPD spectra for zeolite give doublet peaks as shown in Fig. 3. The zeolitic acidity was determined as the area of the high-temperature peak obtained by peak deconvolution.
[b] USY1 and USY2 were commercially available zeolites.
[c] TZ5 and TZ-6 were prepared by immersing 9 g of USY1 in an aqueous solution of $Ti(SO_4)_2$ (0.10 mol/L for TZ-5 and 0.05 m/L for TZ-6, 350 cm^3, pH of about 1) at 50 °C for 0.5 h, followed by filtration, washing by 1000 mL of hot water, drying at 110 °C for 3 h, and calcination at 500 °C for 3 h.

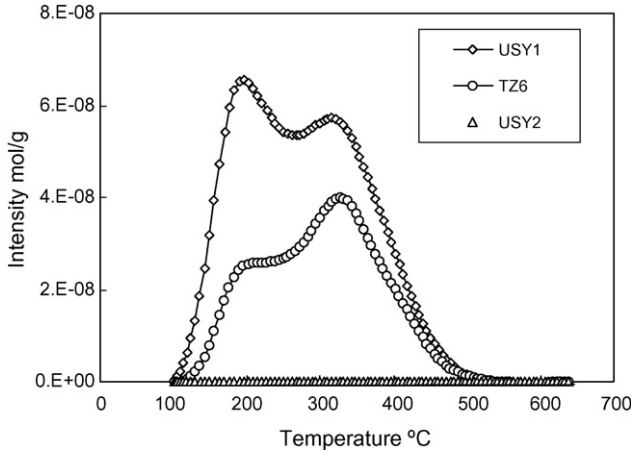

Fig. 2. NH_3-TPD spectra of USY zeolites and $Ti(SO_4)_2$-modified USY (TZ) catalyst.

2.2. Removal of extra-framework Al

Table 1 shows a large discrepancy in the Si/Al ratio between the framework (Si/Al_{fw}) and the bulk (Si/Al_{bk}) for IE2 and IE3. The discrepancy was caused by the deposition of Al species on the surface of the zeolites. Namely, the extracted Al species by IE was not completely removed from the zeolite particles during the washing procedure, and likely formed amorphous Al_2O_3. In fact, the ^{27}Al NMR spectra of most HY zeolites exhibit a peak assigned to octahedrally coordinated Al, although the zeolite framework contains only tetrahedrally coordinated Al [11]. Depending on the final procedure of HY zeolite preparation, for instance steaming or acid treatment, extra-framework Al is preferentially deposited on either the external or internal surface of the zeolite particles [11].

Table 2 [13] shows that the $Ti(SO_4)_2$ modification increased the surface area and pore volume of the starting USY1 zeolite. Fig. 3 compares the pore size distribution profiles of USY1 and TZ6 from Table 2. In addition to the 4-nm-diameter mesopores, USY1 possessed mesopores with diameters larger than 10 nm. These large pores were likely formed by the interconnection of the 4-nm-diameter mesopores during the preparation procedures of USY1. The $Ti(SO_4)_2$ modification further produced mesopores with diameters larger than 10 nm. These changes are attributed to both the extraction of framework Al and to the removal of extra-framework Al. The important roles that mesopores of HY zeolites play in hydrocracking heavy components include the enhancement of pore diffusion as shown previously [14].

When Y zeolite contains extra-framework Al, active hydrogenation components of Mo and Ni are deposited preferentially on the Al_2O_3 surface that is created from the extra-framework Al. Such preferential deposition might hinder the synergy between active hydrogenation sites and acid sites on zeolites and might finally cause coking on the zeolite due to insufficient supply of dissociatively adsorbed hydrogen to the acid sites. In addition, the Al_2O_3 debris might cover or plug the mesopores and thus reduce pore diffusion. There is a dilemma when zeolites with high Si/Al ratios are applied to a support for Mo sulfide catalysts. When zeolite contains extra-framework Al, Mo sulfide catalysts can be highly dispersed on the Al_2O_3 surface [15]. After the removal of the extra-framework Al, however, relatively large MoO_3-like particles are favorably formed on the SiO_2-rich zeolite surface by conventional catalyst preparation methods [15]. To solve this dilemma, we introduced $Ti(SO_4)_2$ modification before Mo loading, because Mo catalysts can be highly dispersed on the TiO_2 surface and yield high catalytic activity after sulfidation. We assumed that the TiO_2 particles would be selectively deposited near the acidic sites of HY zeolites and that the Mo catalysts on TiO_2 would provide synergy between the hydrogenation and cracking active sites.

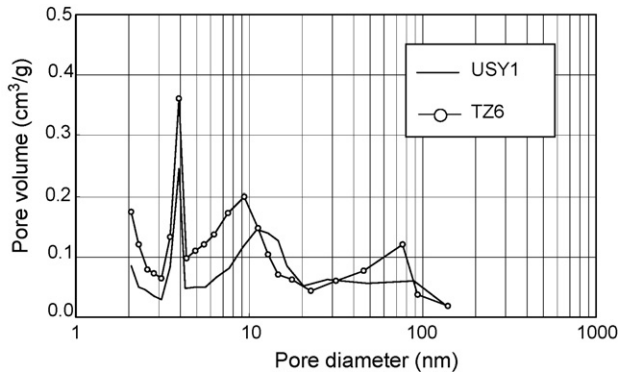

Fig. 3. Change in pore size distribution of USY zeolite with $Ti(SO_4)_2$ modification.

2.3. TiO_2 particles as a support for Mo sulfide catalyst

Various metal oxides have been studied as supports for Co–Mo or Ni–Mo hydrodesulfurization (HDS) catalysts. Among the supports investigated, TiO_2 has often been claimed as a better support for HDS of model compounds and practical feedstocks than most conventionally used γ-Al_2O_3 [15–20]. We previously investigated the orientation and morphology of MoS_2 crystals on γ-Al_2O_3 and TiO_2 particles by using high-resolution transmission electron microscopy (HRTEM) [21–24]. Fig. 4 [22] shows that MoS_2 crystals favor "edge bonding" to the (0 0 1) and (1 0 1) planes of anatase structures due to the epitaxial relationships, whereas only "basal-bonded" MoS_2 crystals are favored on γ-Al_2O_3 surface [21]. We also reported that edge-bonded MoS_2/TiO_2 catalyst possesses

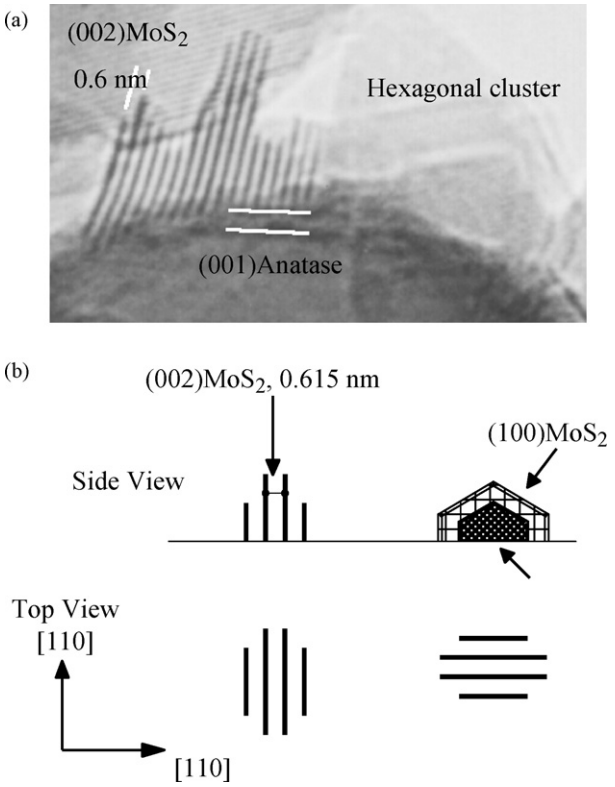

Fig. 4. HRTEM photograph (a) and schematic (b) of MoS_2 crystals on anatase-type TiO_2.

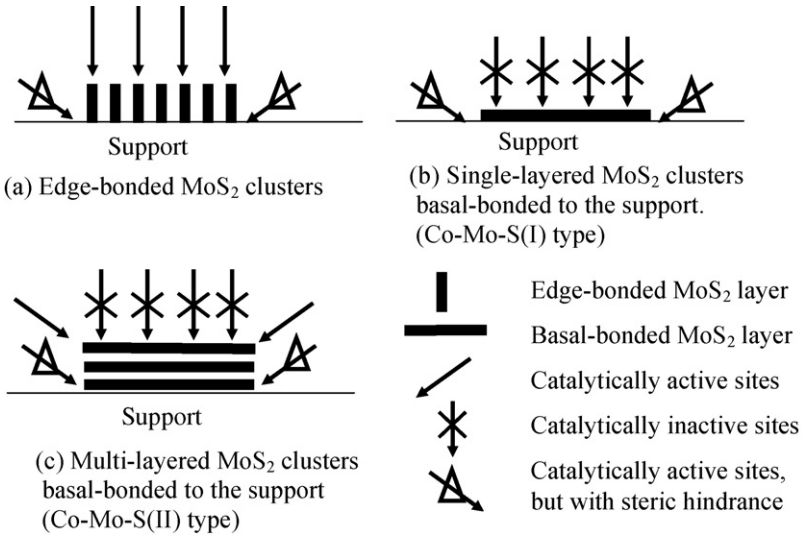

Fig. 5. Orientation and morphology of MoS_2 clusters on supports.

a higher hydrogenation activity than does basal-bonded MoS_2/TiO_2 catalyst [23]. Fig. 5 [23] shows schematics of edge-bonded and basal-bonded MoS_2 catalysts on the supports.

The so-called "Co(Ni)–Mo–S" structure proposed by Topsøe et al. [25] in the late 1980s has been widely accepted as the structural model for the active center of MoS_2-based binary sulfide catalysts. Within the proposed Co–Mo–S structure, however, only a part is considered to function as highly active catalytic sites in practical industrial catalysts [26]. Apparently there are at least two kinds of Co–Mo–S structures; "Co–Mo–S(I)", which has strong electronic interaction with the support, and "Co–Mo–S(II)", which has weak interaction with the support. Co–Mo–S(I) is less catalytically active than Co–Mo–S(II) [27]. Many studies [28–30] report that single-layered MoS_2 catalysts with Co at their edges are Co–Mo–S(I), whereas multi-layered MoS_2 clusters with Co, except the bottom layer, are Co–Mo–S(II). In conclusion, MoS_2 clusters with high aspect ratios (cluster thickness divided by cluster lateral dimension) possess higher intrinsic activities than those with low aspect ratios.

Fig. 5(b) and (c) correspond to the Co–Mo–S(I) and Co–Mo–S(II) structures, respectively. A high degree of sulfidation of Mo on a TiO_2 support has recently been achieved [18,20]. This high degree of sulfidation might be due to the favorable formation of Co–Mo–S(II) structure on TiO_2, because Co–Mo–S(I) structure does not allow complete sulfidation of Mo due to strong interaction with the support. The edge-bonded structure shown in Figs. 4 and 5(a) likely yields the same intrinsic activity as that of Co–Mo–S(II), because the upper edge sites of the edge-bonded MoS_2 clusters that are perpendicular to the support surface supposedly have weak electronic interaction with the support. In fact, our previous study on TiO_2 supported catalysts revealed a high degree of sulfidation of Mo species with edge bonding [23].

The relationship between the morphology and active catalytic sites of MoS_2 clusters has been extensively studied [31–35]. Whitehurst et al. [32] reported steric hindrance that makes the bottom layer of Co–Mo–S less active than the other layers. Because the number of MoS_2 layers that are stacked on γ-Al_2O_3 supported Co–Mo or Ni–Mo catalysts is most likely from one to three, TiO_2 supported Co–Mo or Ni–Mo catalysts are more advantageous compared with γ-Al_2O_3 supported catalysts, particularly in terms of the hydrogenation activity (Fig. 5).

Fig. 6 [13] shows a schematic of the MoS_2 supported USY zeolite catalysts (MTZ catalysts) designed based on the above discussion. The large mesopores enhance the diffusion of heavy components in the feedstocks to the active catalytic sites. The active catalytic sites consist of the acid sites on USY zeolite and hydrogenation active sites on MoS_2. The synergy between these two active sites promotes effective hydrocracking reactions, while suppressing coke formation.

3. Preparation and activity measurements of TZ-based catalyst

3.1. TZ powder supported Mo catalyst (MTZ catalyst)

Mo was loaded by using the equilibrium adsorption method with an aqueous solution of ammonium heptamolybdate.

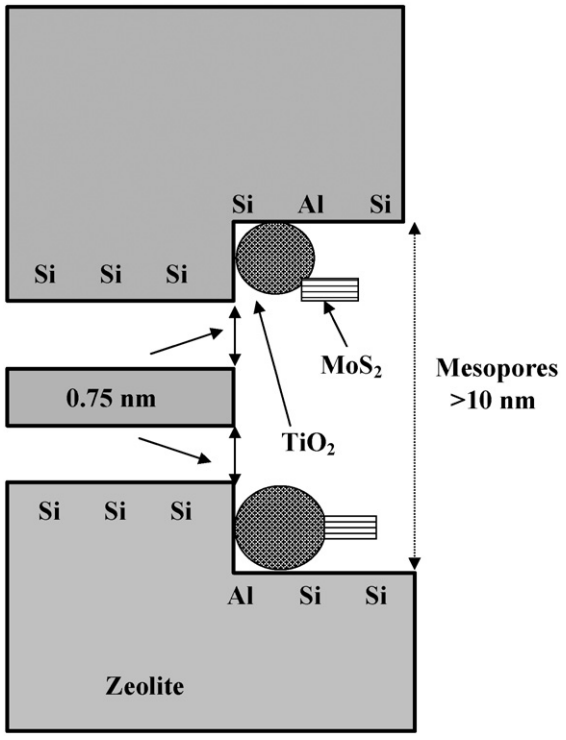

Fig. 6. Schematic of Mo loaded HY zeolite (MTZ) catalyst after $Ti(SO_4)_2$ treatment.

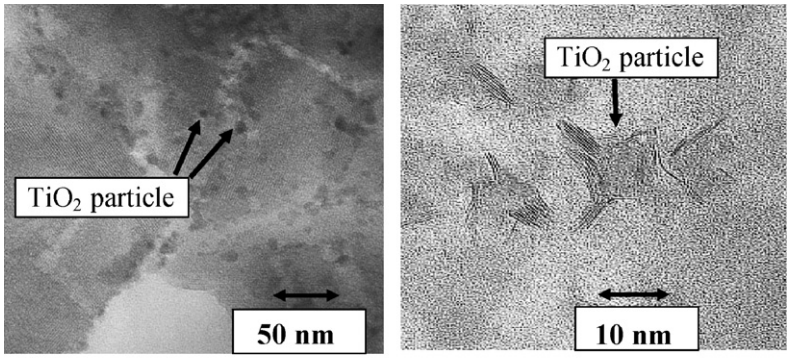

Fig. 7. TEM image of TZ catalyst (a) and Mo loaded TZ (MTZ) catalyst after sulfidation (b).

Table 3
Chemical composition and physical properties of Mo supported USY and TZ catalysts

	Si/Al_{fw}	TiO_2 (%)	Mo (%)	S.A. (m^2/g)	R.C. (%)
MUSY1[a]	4.1	–	4.03	627	79
MUSY2[a]	140	–	0.06	679	84
MTZ5[a]	40	6.5	1.60	804	–[b]
MTZ6[a]	20	8.0	2.26	811	59

[a] MUSY1, MUSY2, MTZ5 and MTZ6 were prepared using the equilibrium adsorption method with USY1, USY2, TZ5 and TZ6, respectively. Adsorption was conducted using an aqueous solution of ammonium heptamolybdate (0.007 mol/L, pH 2) at 50 °C for 24 h. The obtained powder by filtration was dried at 110 °C for 3 h and calcined at 500 °C for 3 h.
[b] Not measured.

This procedure deposited nanometer-sized particles of Mo active species on TiO_2 and minimized the decrease in crystallinity of Y zeolite. Fig. 7(a) [13] shows a TEM image of a TZ catalyst, revealing that TiO_2 particles smaller than 10 nm were dispersed in the zeolite mesopores. Fig. 7(b) shows a TEM image of a Mo-loaded TZ catalyst (MTZ catalyst) after sulfidation, revealing edge-bonded MoS_2 clusters on the TiO_2 surfaces. These TEM images confirm that the MTZ catalyst was prepared according to the schematic shown in Fig. 6. Table 3 [13] compares the properties of MTZ catalysts with those of Mo-loaded USY catalysts (MUSY catalysts). The Mo-loading procedure decreased the crystallinity of the zeolite, although there was no significant deterioration in the crystalline structure because there was no change in the surface area. Note that a very low concentration of Mo (<0.1%) was loaded on MUSY2 with a high Si/Al ratio. This was due to poor interaction between the SiO_2-rich zeolite surface and molybdate anion.

Table 4 [13] compares the catalytic activities of MUSY and MTZ catalysts in the hydrocracking of Arabian Heavy Atmospheric Residue (AH-AR). MUSY1 with the highest acidity exhibited high AR conversion, while resulting in high selectivity to gas and naphtha fractions. In contrast, MUSY2 with almost no acidity exhibited low AR conversion and produced low yields of gas and naphtha fractions. MTZ5 did not exhibit high conversion, but achieved high MD selectivity and low gas and naphtha selectivity, whereas MTZ6 achieved moderate selectivity and high AR and asphaltene conversion. In summary, compared with treatment at a low concentration (0.05 mol/L, TZ6) of $Ti(SO_4)_2$, treatment at a high concentration (0.10 mol/L, TZ5) removed a larger amount of Al from the framework and reduced acidity to a larger extent and produced higher MD selectivity. Note that both MTZ5 and MTZ6 achieved much higher yields of MD fraction and higher conversion of asphaltene than did MUSY1. Fig. 8 [13] compares the distillation profiles of the liquid products obtained in the hydrocracking of AH-AR over MUSY1 and MTZ6. MUSY1 achieved a high yield of liquid product with boiling point below 200 °C, but showed little conversion of the fraction with boiling point exceeded 500 °C, whereas MTZ6 showed conversion of the whole liquid fraction. This indicates that MTZ6 catalyzed hydrocracking reactions of heavy fractions as well as light fractions.

The results in Table 4 and Fig. 8 indicate that MTZ catalysts could accommodate heavy fractions, including asphaltene, whereas MUSY catalysts could not hydrocrack heavy fractions that had a boiling point over 500 °C. This suggests that the large mesoporosity of MTZ catalysts functioned effectively in the

Table 4
Hydrocracking[a] of Arabian Heavy Atmospheric Residue (AH-AR)[b] over Mo supported USY and TZ catalysts

	AR[c] conversion (%)	Yield			Asphaltene[d] conversion (%)
		Gas[c] (%)	Naphtha[c] (%)	MD[c] (%)	
MUSY1	71	17	44	10	43
MUSY2	25	3	2	20	55
MTZ5	45	3	12	30	76
MTZ6	82	5	44	33	80

[a] Hydrocracking reactions were carried out using an autoclave with an inner volume of 140 cm^3. Reaction conditions were as follows: 10 g of AH-AR, 1 g of catalyst (under 200 mesh without presulfidation), initial hydrogen pressure of 9.8 MPa (cold charge), reaction temperature of 410 °C, and reaction time of 6 h.
[b] AH-AR had a density of 0.983 and contained 7.7% asphaltene, 4.2% sulfur and 0.27% nitrogen.
[c] Gas used here consisted of C_1–C_4 hydrocarbons. Naphtha, MD, and AR were determined by simulated distillation using a gas-chromatograph: naphtha with boiling point (b.p.) below 150 °C, MD with b.p. 150–343 °C, and AR with b.p. over 343 °C.
[d] Asphaltene used here was measured as follows. First, 1 g of the liquid product after the naphtha fraction was removed by distillation was mixed with 30 g of heptane and heated to 80 °C. Then, the amount of asphaltene was defined as the weight of the insoluble material measured after filtration, washing by heptane, and drying.

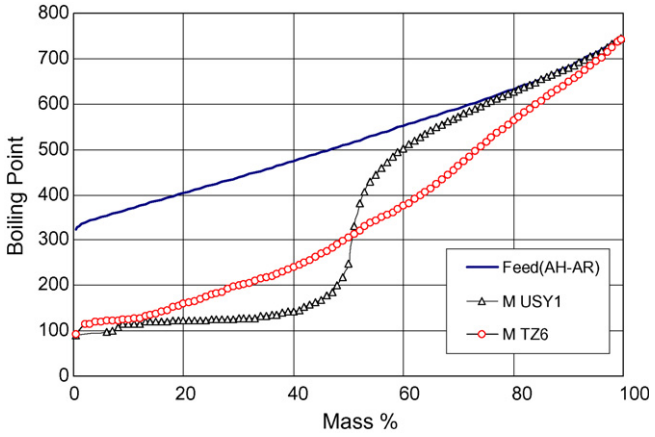

Fig. 8. Distillation curves of feedstock AH-AR and liquid products over MUSY1 and MTZ6.

reaction of large molecules. In addition, the highly dispersed MoS_2 sites on TiO_2 in MTZ catalysts could supply dissociatively adsorbed hydrogen to the acid sites on zeolite to promote hydrocracking and to suppress coking, whereas in MUSY1, the "synergy" between the hydrogenation active sites and acid sites did not function effectively. The lower MD selectivity of MTZ6 compared with MTZ5 is probably due to over-cracking of the MD fraction caused by the high density of acid sites on MYZ6.

3.2. MTZ-based Ni–Mo extrudate-type catalysts (NiMo/MTZ catalysts)

To evaluate the catalytic performance of practical NiMo/MTZ catalysts in a continuous flow-type reactor with fixed catalyst bed, we prepared extrudate-type catalysts by using MTZ powders. Table 5 [36] lists the properties of MTZ and AZ powders used for the preparation of these extrudate-type catalysts. AZ powders were prepared by immersing USY1 in aqueous solutions of H_2SO_4 instead of $Ti(SO_4)_2$. TZ-N1 and TZ-N2 were prepared so that the properties would respectively correspond to those of TZ5 and TZ6. AZ-1 and AZ-2 were prepared by treating USY1 with aqueous H_2SO_4 solutions to clarify the effects of the $Ti(SO_4)_2$ modification followed by Mo loading. Note that the preparation conditions used for TZ-N1 and TZ-N2 in Table 5 differed from those used for TZ5 and TZ6 in Table 2, because the conditions required for the large-scale preparation of TZ (60 g) differed from those for small-scale production (9 g). Although the crystallinity of TZ-N was slightly lower than that of TZ, the framework Si/Al ratio of TZ-N corresponded to that of TZ. The Al^{VI} percentage obtained from ^{27}Al-MAS-NMR is an index for the amount of extra-framework Al. As shown in Table 5, both $Ti(SO_4)_2$ and H_2SO_4 treatments were effective in removing the extra-framework Al and in increasing the mesoporosity.

Table 6 [36] shows the properties of the Ni–Mo supported extrudate-type catalysts prepared using USY1, TZ-N and AZ powders, and Al_2O_3 binders. All the catalysts had similar chemical composition and physical properties, because about half of each catalyst was the same γ-Al_2O_3. Table 7 [36] compares the catalytic

Table 6
Properties of Ni–Mo supported extrudate-type catalysts

	NiO (%)	MoO_3 (%)	Meso PV (cm^3/g)	S.A. (m^2/g)
NiMo/USY1[a]	3.7	14.0	0.55	340
NiMo/MTZ-N1[a]	3.7	15.0	0.55	399
NiMo/MTZ-N2[a]	3.8	14.2	0.45	369
NiMo/AZ-1[a]	3.7	14.0	0.50	357
NiMo/AZ-2[a]	3.7	14.3	0.51	350

[a] All the extrudate-type catalysts were prepared as follows. First, 10 g of zeolite powders (USY1, MTZ-N or AZ) were mixed with a small amount of water and 13.33 g of commercially available Al_2O_3 binder (pseudo-boemite, Al_2O_3 content of 75%) so that the final catalyst would contain 50% of zeolite. Then, the paste was molded in 1/32-inch-diameter cylinders, followed by drying at 120 °C for 2 h and calcining at 550 °C for 2 h. The Ni and Mo loading was conducted using the one-step incipient wetness impregnation method with aqueous solutions of $Ni(NO_3)_2$ and $(NH_4)_6Mo_7O_{24}$. The impregnated catalysts were then dried at 120 °C for 2 h and calcined at 550 °C for 2 h.

Table 7
Hydrocracking[a] of hydrotreated Arabian Light Atmospheric Residue (AL-AR-HDM)[b] over Ni–Mo extrudate-type catalysts using an autoclave

	AR conversion (%)	Yield		
		Gas (%)	Naphtha (%)	MD (%)
NiMo/USY1	45	3.6	15.5	31
NiMo/MTZ-N1	38	3.8	8.5	32
NiMo/MTZ-N2	54	4.1	15.5	38
NiMo/AZ-1	27	3.1	5.9	25
NiMoAZ-2	50	4.1	13.9	36

[a] Hydrocracking reaction conditions were the same as those in Table 4.
[b] AL-AR used here was hydrotreated to reduce the sulfur and metal content before use. Properties of AL-AR-HDM were density of 0.941 and a composition of 90% AR fraction, 1.7% sulfur, 0.17% nitrogen, 1.0% asphaletene, and 12 wtppm metal (Ni, V).

Table 5
Properties of Mo supported $Ti(SO_4)_2$ modified zeolite (MTZ) and H_2SO_4 treated zeolite (AZ) catalysts

	TiO_2 (%)	Mo (%)	Si/Al_{fw}	S.A. (m^2/g)	Meso PV (cm^3g)	R. C. (%)	Acidity (mmol/g)	$Al^{VI,a}$ (%)
USY1[b]	–	–	2.9	586	0.075	83	0.80	38
MTZ-N1[c]	6.3	1.4	40	763	0.102	20	0.50[e]	24
MTZ-N2[c]	13.7	2.1	18	777	0.106	47	0.94[e]	34
AZ-1[d]	–	–	33	628	0.090	28	0.33	10
AZ-2[d]	–	–	18	795	0.100	61	0.73	–[f]

[a] Percentage value of octahedral Al measured by ^{27}Al-MAS-NMR.
[b] USY1 was the same commercially available zeolite as that in Table 2. Differences in the properties between Tables 2 and 5 are due to the different lots used and/or different analytical methods.
[c] MTZ-N1 and MTZ-N2 were prepared using the equilibrium adsorption method with TZ-N1 and TZ-N2, respectively. TZ-N1 and TZ-N2 were prepared by immersing 60 g of USY1 in an aqueous solution of $Ti(SO_4)_2$ (0.05 mol/L for TZ-N1 and 0.04 mol/L for TZ-N2, 2.5 L) first at 30 °C for 2 h and then at 45 °C for 2 h, followed by filtration and washing by 100 cm^3 of H_2SO_4 (0.1 mol/L) and ion-exchanged water until no sulfate ion was detected. The obtained powder was then dried at 120 °C for 3 h and calcined at 500 °C for 3 h. Equilibrium adsorption of Mo was conducted using an aqueous solution of ammonium heptamolybdate (0.007 mol/L, pH 2) at 50 °C for 4 h. The obtained powder by filtration was again dried at 120 °C for 3 h and calcined at 500 °C for 3 h.
[d] AZ-1 and AZ-2 were prepared by immersing USY1 in aqueous solutions of H_2SO_4 (0.16 mol/L for AZ-1 and 0.13 mol/L for AZ-2), followed by the same washing, drying, and calcination procedures as those for TZ-N.
[e] Values for TZ-N1 and TZ-N2.
[f] Not measured.

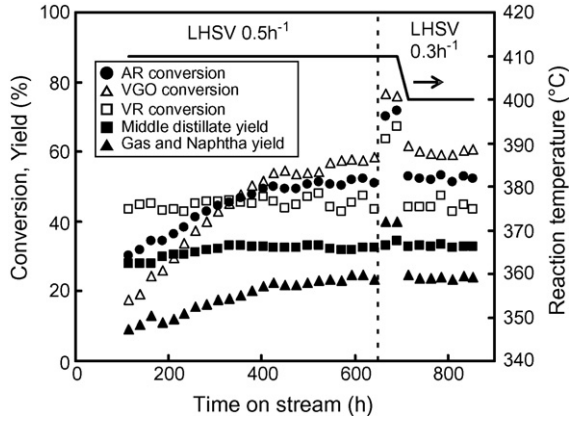

Fig. 9. Change in catalytic activity of NiMo/MTZ-N1 with time on stream. Catalyst volume, 80 cm^3; H_2 pressure, 13.8 MPa; gas/oil, 2000 NL/L; Feed, AL-AR-HDM in Table 7. Catalyst was presulfided with light gas oil (LGO) containing dimethyldisulfide (S = 3 wt%) at 250 °C for 11 h.

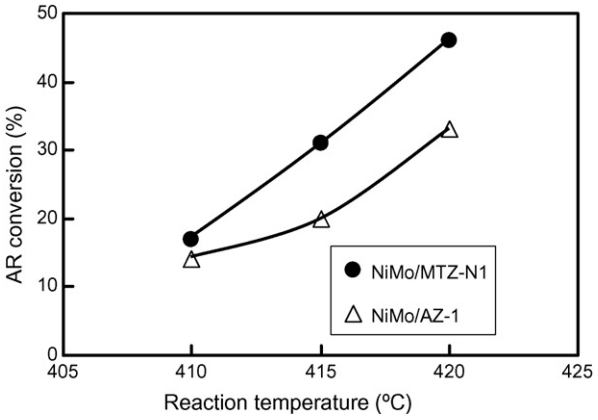

Fig. 11. Comparison of catalytic activity of NiMo/MTZ-N1 and NiMo/AZ-1 reactions were conducted using the same reactor and under the same conditions as described in Fig. 9. Feed used was hydrotreated Kuwait Atmospheric residue (Kw-AR-HDM) with density of 0.936, and composition of 92% AR fraction, 1.1% sulfur, 0.19% nitrogen, 1.3% asphaltene, and 26 wtppm metal (Ni, V).

activities of the extrudate-type catalysts in Table 6 that were evaluated using an autoclave. The feedstock, Arabian Light Atmospheric Residue (AL-AR), had been pre-treated to reduce the sulfur and metal contents because in practical refineries, hydrocracking catalysts are most likely placed after the hydrodemetallation (HDM) and HDS catalyst beds. Compared with NiMo/USY1, both NiMo/MTZ-N2 and NiMo/AZ-2 with relatively low Si/Al ratios yielded higher AR conversion and higher MD yields (Table 7). NiMo/MTZ-N1 and NiMo/AZ-1 with relatively high Si/Al ratios showed lower AR conversion but higher selectivity to MD fraction. These results indicate that both $Ti(SO_4)_2$ and H_2SO_4 treatments could improve the hydrocracking of AR and the selectivity to MD fraction. The selectivity, which is the most important characteristic of the catalyst, was superior when treated with higher concentrations of $Ti(SO_4)_2$ (NiMo/MTZ-N1) or H_2SO_4 (NiMo/AZ-1) than with lower concentrations (NiMo/MTZ-N2 and NiMo/AZ-2). In summary, these reaction results demonstrate that the zeolite-based powders were well dispersed in alumina matrix and that they maintained their catalytic performance in the extrudate-type catalysts. Note that the difference in the catalytic activity among the Ni–Mo extrudate-type catalysts was much smaller than that among the powder catalysts. This was because all the extrudate-type catalysts contained Ni–Mo sulfide with high hydrogenation activity and possessed large mesoporosity due to the high amount of γ-Al_2O_3 component.

Fig. 9 [36] shows an example of the catalytic activity tests in a continuous flow-type reactor with a fixed catalyst bed. After the presulfiding, the reaction was started at 250 °C and then the temperature was gradually increased to 410 °C over a period of 100 h to prevent the catalyst from coking. This procedure resulted in the seeming "recovery" of the catalyst performance, because basic compounds in the feedstock covered the active catalytic sites at the beginning of the reaction when the reaction temperature was low. It took about 400 h for the catalyst to reach stable activity, after which almost constant yields of gas, naphtha and MD fractions were obtained until the end of the reaction. Similar behavior was observed for all the catalysts tested. The AR conversion values at 410 °C and LHSV of 0.5 h^{-1} decreased in the following order: NiMo/MTZ-N2 (67%) > NiMo/USY1 (57%) > NiMo/MTZ-N1 (51%). This order is the same as that obtained using an autoclave (Table 7).

Fig. 10 [36] plots the relationship between AR conversion and MD yield over NiMo/MTZ-N1, NiMo/MTZ-N2 and NiMo/USY. The

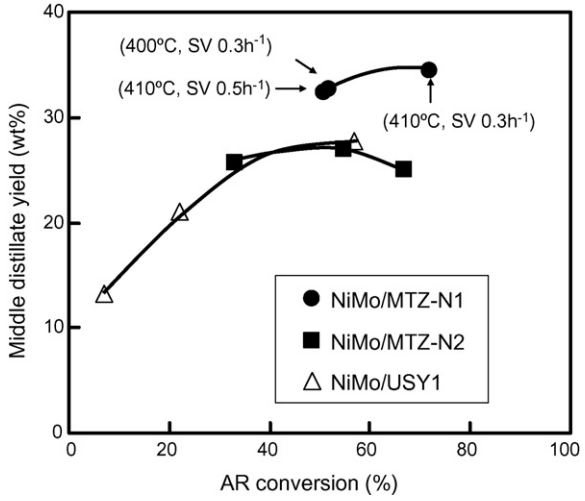

Fig. 10. AR conversion vs. middle distillate (MD) yield over NiMo/MTZ and NiMo/USY. Reactions were conducted using the same reactor and under the same conditions as described in Fig. 9. Feed used was AL-AR-HDM in Table 7.

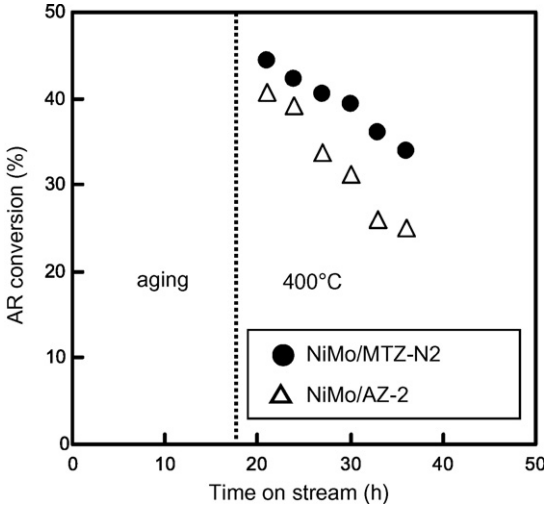

Fig. 12. Accelerated deactivation tests of NiMo/MTZ-N2 and NiMo/AZ-2 using a micro-plant with a reactor volume of 15 cm^3. Feed used was AL-AR-HDM in Table 7.

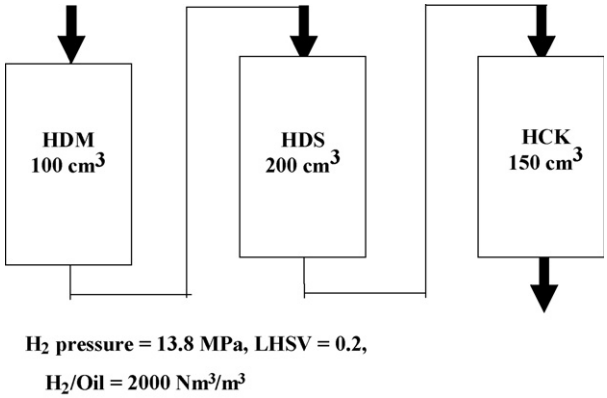

Fig. 13. Schematic of the large-scale bench plant used for long-term catalyst aging tests. Feed used was Kw-AR with density of 0.977 and composition of 95% AR fraction, 4.4% sulfur, 0.24% nitrogen, 3.5% asphaletene and 81 wtppm metal (Ni, V). Reaction temperature of HDM + HDS sections was controlled so that the sulfur content in the product oil was 0.3%, whereas that of the HCK section was kept at 400 °C.

NiMo/MTZ-N1 yielded higher selectivity to MD compared with NiMo/MTZ-N2 and NiMo/USY1. These results are consistent with those shown in Table 7.

Fig. 11 [34] compares the conversion of hydrotreated Kuwait Atmospheric Residue (Kw-AR-HDM) over NiMo/MTZ-N1 and NiMo/AZ-1 obtained using the same reaction system as shown in Fig. 9. In the hydrocracking reaction of Kw-AR-HDM, which contained larger amounts of heavy components with low reactivity than AL-AR-HDM, these two catalysts exhibited stable activity for more than 1000 h when the experiments were ended, although the reaction temperature for the same AR conversion was 10 °C higher than that for AL-AR-HDM. At each reaction temperature, NiMo/MTZ-N1 yielded higher conversion than did NiMo/AZ-1. No difference in the selectivity to MD fraction was observed between the two catalysts at the same AR conversion.

Despite relatively higher Si/Al ratios (i.e., lower acidity), MTZ catalysts yielded higher AR conversion than did AZ catalysts as shown in Fig. 11. This higher conversion was attributed to the higher hydrogenation activity of MTZ catalysts compared with AZ catalysts. The highly dispersed Mo sulfide catalysts near hydrocracking active sites functioned effectively in suppressing the coke formation, thus resulting in the higher AR conversion. This discussion was supported by the accelerated deactivation tests shown in Fig. 12 [36]. In the experiments for Fig. 12, the temperature for the catalyst bed was increased to 400 °C right after the presulfiding. Although the AR conversion values over both catalysts rapidly decreased, the decrease over NiMo/MTZ-N2 was less steep than that over NiMo/AZ-2.

MTZ catalysts were designed to have the following advantages compared with conventional USY catalysts by producing the structure shown in Fig. 6.

1. Large mesopores that enhance the diffusion of large molecules.
2. Less acidity that hinders the over-cracking reactions to gas and naphtha fractions.

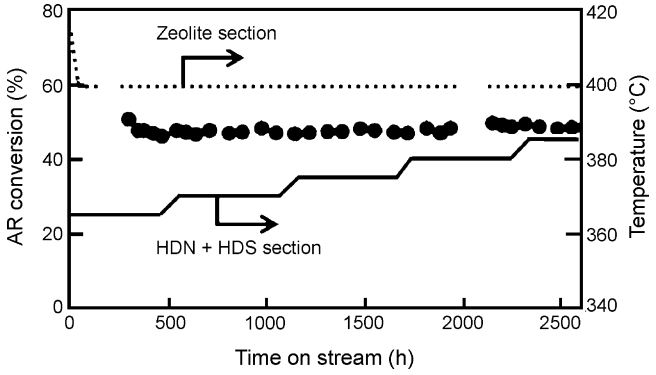

Fig. 14. AR conversion with time on stream in long-term catalyst aging test.

3. High hydrogenation activity linked to acid sites that promote the hydrocracking of heavy fraction and suppress the coke formation.

Note that AZ catalysts also have the first two advantages listed above. The results reported in this current study indicate that these first two advantages are quite effective for achieving high MD selectivity (Table 7 and Fig. 10). The third advantage is the particular advantage that MTZ catalysts have over AZ catalysts, and was shown effective for achieving high AR conversion due to the suppression of the initial catalyst deactivation (Fig. 12), although its effectiveness in terms of MD selectivity remains unclear.

3.3. Long-term life test of NiMo/MTZ catalyst

As the next step in the development of practical hydrocracking catalysts, NiMo/MTZ was prepared on a large scale, and then tested in a bench-scale plant to evaluate for the long-term life behavior of the catalyst. Fig. 13 [37] shows the reaction system in which HDM and HDS reactors contained commercially available HDM and HDS catalysts, and the hydrocracking section was loaded with NiMo/MTZ. The reaction conditions for the hydrocracking section were similar to those used for the activity tests shown in Fig. 9.

Fig. 14 [37] shows the changes in reaction temperature and AR conversion with time on stream. The temperature for the HDM and HDS section was increased every 500–550 h to compensate for the gradual catalyst deactivation. The AR conversion was stable at 47% up to 2600 h, despite keeping the temperature at 400 °C. MD selectivity was maintained at 30% during the entire test. Table 8 [37] shows the properties of the products obtained in this catalyst life test. The quality of MD (kerosene and diesel) was excellent, as evidenced by the high smoke point and high cetane number in addition to low sulfur and nitrogen content. The density of AR was lower than that obtained from conventional AR HDS processes, indicating that the AR obtained over the present hydrocracking process would be a good feedstock for FCC processes. Further study to confirm the superiority of the present MTZ catalysts is underway using deasphalted oil (DAO) as the feedstock [38].

Table 8
Properties of the products obtained in the catalyst life test

	Yield (%)	Density (g/cm^3)	Sulfur (ppm)	Nitrogen (ppm)	Smoke point (mm)	Cetane index	CCR[a] (%)
Kerosene	16.0	0.809	17	3	21.0	–	–
Diesel	13.2	0.844	33	6	–	55.8	–
AR	50.7	0.908	3000	1000	–	–	5.6

[a] Conradson carbon residue.

4. Conclusion

$Ti(SO_4)_2$ modified USY zeolite-based NiMo hydrocracking catalysts were designed and developed to increase the yields of transportation fuel, particularly MD fraction, from heavy petroleum feedstocks. The catalysts showed high AR conversion, high selectivity to MD fraction, and good stability up to 2600 h in the bench-scale test. Large mesoporosity and controlled acidity were found effective for high selectivity to MD fraction. The synergy between hydrogenation active sites originating from MoS_2 on TiO_2 and acid sites on USY zeolite effectively suppressed the initial catalyst deactivation caused by coking.

Acknowledgements

This study was partly carried out as a research project of Japan Cooperation Center, Petroleum with a subsidy from the Ministry of Economy, Trade and Industry.

References

[1] World Energy Outlook 2007, International Energy Agency, 2007.
[2] I.E. Maxwell, Catal. Today 1 (1987) 385.
[3] F. Morel, S. Kressmann, V. Harle, S. Kasztelan, Stud. Surf. Sci. Catal. 106 (1997) 1.
[4] K. Seimiya, M. Hashimoto, S. Suzuki, M. Kameyama, K. Nita, Sekiyu Gakkaishi (J. Jpn. Petrol. Inst.) 33 (1990) 52.
[5] K. Sato, Y. Iwata, T. Yoneda, A. Nishijima, Y. Miki, H. Shimada, Catal. Today 45 (1998) 367.
[6] J. Ward, Fuel Process. Technol. 35 (1993) 55.
[7] H. Shimada, S. Yoshitomi, T. Sato, N. Matsubayshi, M. Imamura, Y. Yoshimura, A. Nishijima, Stud. Surf. Sci. Catal. 106 (1997) 115.
[8] C. Leyva, M.S. Rana, F. Trejo, J. Ancheyta, Ind. Eng. Chem. Res. 46 (2007) 7448.
[9] M.S. Rana, F. Trejo, J. Ancheyta, S.K. Maity, P. Rayo, Catal. Today 130 (2008) 411.
[10] US Patent 6,682,650 (2004).
[11] K. Sato, Y. Nishimura, M. Imamura, N. Matsubayashi, H. Shimada, Micropor. Mesopor. Mater. 59 (2003) 133.
[12] D.W. Breck, Zeolites Molecular Sieves, John Wiley & Sons, New York, 1974, p. 94.
[13] K. Honna, Y. Araki, T. Enomoto, M. Yoshimoto, H. Shimada, Sekiyu Gakkaishi (J. Jpn. Petrol. Inst.) 46 (2003) 249.
[14] K. Sato, Y. Nishimura, K. Honna, N. Matsubayashi, H. Shimada, J. Catal. 200 (2001) 288.
[15] H. Shimada, T. Sato, Y. Yoshimura, J. Hiraishi, A. Nishijima, J. Catal. 110 (1988) 275.
[16] S. Matsuda, A. Kato, Appl. Catal. 8 (1983) 149.
[17] K.Y.S. Ng, E. Gulari, J. Catal. 95 (1985) 33.
[18] Y. Okamoto, A. Maezawa, T. Imanaka, J. Catal. 120 (1989) 29.
[19] R.G. Leliveld, A.J. van Dillen, J.W. Geus, D.C. Koningsberger, J. Catal. 171 (1997) 115.
[20] S. Yoshinaka, K. Segawa, Catal. Today 45 (1998) 293.
[21] Y. Sakashita, Y. Araki, H. Shimada, Appl. Catal. A215 (2001) 101.
[22] Y. Sakashita, Y. Araki, K. Honna, H. Shimada, Appl. Catal. A197 (2000) 247.
[23] Y. Araki, K. Honna, H. Shimada, J. Catal. 207 (2002) 361.
[24] H. Shimada, Catal. Today 86 (2003) 17.
[25] H. Topsøe, B.S. Clausen, R. Candia, C. Wivel, S. Mørup, J. Catal. 68 (1981) 433.
[26] H. Topsøe, B.S. Clausen, F.E. Massoth, Hydrotreating catalysis, in: J.R. Anderson, M. Boudart (Eds.), Catalysis-Science and Technology, 11, Springer-Verlag, Berlin/Heidelberg, 1996.
[27] R. Candia, O. Sørensen, J. Villadsen, N.-Y. Topsøe, B.S. Clausen, H. Topsøe, Bull. Soc. Chim. Belg. 93 (1984) 763.
[28] S.M.A.M. Bouwens, F.B.M. van Zon, M.P. van Dijk, A.M. van der Kraan, V.H.J. de Beer, J.A.R. van Veen, D.C. Koningsberger, J. Catal. 146 (1994) 375.
[29] H. Topsøe, B.S. Clausen, N.-Y. Topsøe, P. Zeuthen, Stud. Surf. Sci. Catal. 53 (1990) 77.
[30] S. Eijsbouts, Appl. Catal. A158 (1997) 53.
[31] M. Daage, R.R. Chianelli, J. Catal. 149 (1994) 414.
[32] D.D. Whitehurst, T. Isoda, I. Mochida, Adv. Catal. 42 (1998) 345.
[33] M. Vrinat, M. Breysse, C. Geantet, J. Ramirez, F.E. Massoth, Catal. Lett. 26 (1994) 25.
[34] S. Kasztelan, L. Jalowiecki, A. Wambeke, J. Grimblot, J.P. Bonnelle, Bull. Soc. Chim. Belg. 96 (1987) 1003.
[35] F.E. Massoth, G. Muralidhar, in: Proceedings of the Fourth International Conference on the Chemistry and Uses of Molybdenum, Climax Molybdenum Co., 1982, p. 343.
[36] T. Enomoto, H. Aizono, H. Ueki, Y. Hashimoto, N. Ohshio, K. Honna, M. Yoshimoto, H. Shimada, Sekiyu Gakkaishi (J. Jpn. Petrol. Inst.) 47 (2004) 239.
[37] N. Ohshio, T. Enomoto, K. Honna, H. Ueki, Y. Hashimoto, H. Aizono, M. Yoshimoto, H. Shimada, Fuel 83 (2004) 1895.
[38] M. Ushio, J. Futigami, R. Kuroda, T. Ida, Y. Yamahata, K. Hayashida, T. Kameoka, in: Proceedings of the Abstract of the Fifth Tokyo Conference on Advanced Catalytic Science and Technology, 2006, p. 68.